THE JOURNAL OF PHYSICAL CHEMISTRY B
A JOURNAL OF THE AMERICAN CHEMICAL SOCIETY

pubs.acs.org/JPCB

Article

Anomalously Small Reorganization Energy of the Half Redox Reaction of Azurin

Setare M. Sarhangi and Dmitry V. Matyushov*

Cite This: J. Phys. Chem. B 2022, 126, 3000−3011

Read Online

ACCESS | Metrics & More | Article Recommendations | Supporting Information

ABSTRACT: Small values of the reorganization energy, 0.2−0.3 eV, were reported by electrochemical kinetic measurements for the half redox reaction of the redox-active protein azurin. This theoretical study explores possible mechanisms for the low activation barrier for electrochemical protein electron transfer: (1) electronic polarizability of the active site, (2) altering protonation states of far-away histidine residues not directly connected to the active site, and (3) a partial desolvation of the protein when attached to the electrode. The last mechanism provides the most robust explanation of the observations. Constraints imposed by the protein fold on its ability to sample the configuration space lead to the breakdown of the fluctuation−dissipation relation (FDR) and a strong separation of the Stokes-shift and variance reorganization energies. The resulting nonergodic kinetic reorganization energy observed experimentally is significantly lowered compared to predictions of standard models based on Gibbsian statistics and the FDR. The fast rate of protein electron transfer is directly related to the ability of the protein scaffold to maintain nonequilibrium statistics of electrostatic fluctuations projected on the electron-transfer reaction coordinate.

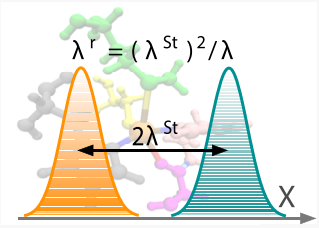

INTRODUCTION

Electron transport in biological energy chains must proceed with sufficient speed to allow an efficient operation of the entire chain. A sequence of electron hops leading to the cross-membrane charge separation is usually viewed as a fast component of the overall charge transport, and it is the catalytic reaction that typically appears to be the slowest and rate-determining step of the charge-transfer chain. Electron transport is therefore viewed as the least challenging component of bioenergetics. Because many electron-transfer steps proceed with small reaction free energy,[1] the kinetics is described by the normal region of the Marcus theory[2] with the barrier mostly determined by the reorganization energy of electron transfer λ to which a "generic" value $\simeq 0.8$ eV is often assigned.[3] Values in this range are indeed found experimentally when the driving force (the negative of the reaction free energy ΔF_0) is varied. The reorganization energy is then obtained by fitting the activation barrier $\Delta F^{\dagger}$ to the Marcus bell-shaped function

$$\Delta F^{\dagger} = \frac{(\lambda^{r} + \Delta F_0)^2}{4\lambda^{r}} \quad (1)$$

In this equation, the "reaction" reorganization energy λ^{r} specifies its origin in kinetic measurements (see below for a precise definition).

Reorganization energies λ^{r} are often obtained from kinetic studies when both the donor and acceptor belong to the same protein molecule, such as in Ru-modified metalloproteins in which an electron is injected to the metal-containing active site from a photoexcited $Ru(bpy)_2$ complex chemically linked to the protein surface.[4] Kinetics of electron transfer can be alternatively studied by electrochemistry when the electron is exchanged between the metal electrode and the active site in a half redox reaction. A number of such studies have reported reorganization energies of half reactions significantly lower than those obtained from solution kinetic measurements. The blue copper protein azurin studied here is a good example of such a discrepancy: while solution studies[5,6] (labeled "solution" in Table 1) have shown the reorganization energies of the order 0.7−0.8 eV, a number of electrochemical experiments[7−11] (labeled "half" for a half redox reaction in Table 1) have reported much lower values of 0.2−0.3 eV. Solution experiments, requiring an attachment of a redox site to the surface of the protein, are affected by the exposure of that redox site to water, thus resulting in its dominance in the overall reorganization energy of a redox reaction.[12] Electrochemistry[8−11] and electrochemical scanning tunneling microscopy[7,13] can potentially provide more reliable estimates of medium reorganization of the protein-water thermal bath in response to altering the oxidation state of the active site. The experimental results presented in Table 1 are compared with calculations of half reactions[14−16] from trajectories produced by molecular dynamics (MD) simulations.

Received: January 15, 2022
Revised: March 27, 2022
Published: April 15, 2022

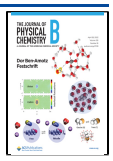

https://doi.org/10.1021/acs.jpcb.2c00338
J. Phys. Chem. B 2022, 126, 3000−3011

Table 1. Reorganization Energies (eV) for Electrochemical (Half) and Solution Electron-Transfer Reactions in Azurin from Experiment and Calculations

source	λ^{St}	λ_{Ox}	λ_{Red}	λ^{r}	refs
experiment (half)[a]				0.3	9, 10
experiment (half)				0.21−0.25	11
experiment (half)[b]				0.2−0.4	8
experiment (half)				0.35−0.45	7
experiment (half)				0.13	13
experiment (solution)				0.8	5
experiment (solution)				0.78	6
calculations (half)[c,d]	0.96(300)	1.35	1.44	0.66	present
calculations (half)	1.05(100)				14
calculations (half)	0.9(0.16)				15
calculations (half)[e]	1.2−1.4(0.7)				16

[a]Experiments are done with *Pseudomonas aeruginoza* azurin[18] (PDB 4AZU). [b]λ is found to continuously increase from 0.2 to 0.4 eV with the increase in the thickness of the surface assembled monolayer. [c]λ^{r} is calculated by combining $\lambda = (\lambda_{Ox} + \lambda_{Red})/2$ with λ^{St} in eq 6. [d]The numbers in parentheses indicate the trajectory length in ns. [e]DFT/MM calculations for plastocyanin in TIP3P water.

Significant discrepancies between different experimental sources of the electron-transfer reorganization energy in proteins call for a theoretical explanation, which is sought in this article. More generally, the problem of protein electron transfer, with its sufficient experimental database and many theoretical algorithms developed to perform detailed calculations, presents itself as a good testing platform for formulating general principles of activated kinetics in enzymes and the linkage between chemical dynamics and the heterogeneous protein-water thermal bath. Given that electrostatics is essential for most enzymatic reactions,[17] the nonergodic sampling of electrostatic fluctuations by protein electron transfer presents itself as a general principle for lowering the activation barrier of activated transitions. We find below that it is the protein component of the thermal bath that allows such a nonergodic sampling of the configuration space.

A number of early experiments by Frauenfelder and coworkers have shown that binding kinetics of simple diatomics to myoglobin is highly heterogeneous, with many activation barriers sampled through slow exploration of the conformational landscape by a single protein.[19,20] Such heterogeneity of reaction rates was confirmed for slow recombination rates in bacterial photosynthesis[21] and in a number of more recent single-molecule experiments.[22−26] The main result of these studies is the concept of dynamic disorder[27] suggesting that the active space of a reacting enzyme is a small sub-ensemble of a large number of possible states. Most of them are inactive and the enzymatic reaction can only occur from a small subspace of "hot" states.[28,29] The time of transition between distinct functional states can be very long, from milliseconds up to 10^2 s.[30−32]

The presence of a large ensemble of activation barriers for a given reaction implies a certain separation of time scales. There is a subset of fast thermal bath motions, and their thermal fluctuations lead to activated transitions across the activation barrier. However, other fluctuations remain slow and are effectively dynamically frozen on the time scale of each individual reaction. Their subsequent relaxation, on a much longer time scale, leads to the observed heterogeneity of the reaction rates. The distribution of reaction rates and of the midpoint potential (∼45 mV) could be recorded in a single-molecule study of the redox reaction between azurin and hexacyanoferrate.[25] The long reaction time, ∼0.1 s, allowed the reacting system to sample transitions between individual substates. The very existence of such substates poses a fundamental question of how to describe faster reactions, on the nanosecond time scale, when these slow conformational motions become dynamically arrested and sampling of the configuration space by the protein becomes incomplete.

The separation of time scales between nuclear motions promoting activated transitions and those responsible for the rate heterogeneity implies that equilibrium statistics is not established for the barrier crossing phenomena. One has to address the question of whether the nonequilibrium statistics of the thermal bath has any effect on the reaction rate and/or creates any advantages for the catalytic action of the redox enzyme. It is clear that if the time scales of slow motions far exceed those of the reaction, the reaction kinetics can be treated by averaging the population dynamics over the heterogeneous distribution of alternative configurations. If this extreme separation of time scales does not occur, this recipe does not apply and one has to think about the problem in terms of "continuous ergodicity breaking"[33] when the reaction window establishes the cutoff frequency within the spectrum of the bath modes affecting the reaction.[34]

The nonequilibrium character of bath fluctuations can also affect statistical laws connecting different moments of observable properties known as fluctuation−dissipation relations (FDRs). Protein electron transfer becomes the primary testing ground for such violations of the FDR because traditional models of electron transfer[2] are constructed assuming the validity of these relations.[34]

The rate of electron transfer between electronic states localized at specific molecular sites is determined as Golden rule tunneling achieved when electronic resonance is produced by thermal fluctuations of the medium.[35] Because most of the electron-medium coupling is established through long-range electrostatics,[36] statistics of the donor−acceptor energy gap X (explained in more detail below) is Gaussian. The probability of tunneling scales with a Gaussian probability of the resonance condition $X = 0$

$$k_{ET} \propto V^2 \exp\left[-\frac{\langle X\rangle^2}{2\sigma_X^2}\right] \tag{2}$$

where $\langle X\rangle$ is the average donor−acceptor energy gap[37] and σ_X^2 is its variance; V is the electron-transfer coupling decaying exponentially with the donor−acceptor distance.[4]

The standard Marcus eq 1 is obtained in two steps. One applies the FDR to connect the variance to the reorganization energy λ

$$\sigma_X^2 = 2\lambda k_B T \tag{3}$$

https://doi.org/10.1021/acs.jpcb.2c00338
J. Phys. Chem. B 2022, 126, 3000−3011

followed by splitting the average energy gap into the reorganization energy and the reaction free energy: $\langle X\rangle = \lambda + \Delta F_0$. Note that even though both components in this sum carry the meaning of free energies in linear solvation theories, the total is the vertical energy gap, thus requiring the entropy components to cancel out in the sum. When the FDR and the Gaussian statistics are applied, one finds $\lambda = \lambda^r$ and all routes to the reorganization energy converge to a single parameter. An alternative route to λ, often employed in numerical simulations because of lower numerical cost, is through the difference of first moments of the energy gap in the initial, $i = 1$, and final, $i = 2$, reaction states. This route, closely related to the Stokes shift in spectroscopy, leads to the Stokes-shift reorganization energy

$$\lambda^{St} = \frac{1}{2}|\langle X\rangle_1 - \langle X\rangle_2| \tag{4}$$

The FDRs require all three reorganization energies to be identical, $\lambda^r = \lambda = \lambda^{St}$.

The often adopted generic value of the reorganization energy[3] ≃0.8 eV is justified by the notion that proteins are on average nonpolar media as supported by dielectric measurements of protein powders. The standard argument then suggests that the protein matrix provides a buffering medium to push water away from the active site to lower the solvent reorganization energy. An additional argument for the low overall λ invokes small structural changes of the active site leading to a low reorganization energy of intramolecular vibrations.[38−41] This second requirement is only relevant when the frequencies of intramolecular vibrations ν_i coupled to electron transfer are in the classical domain $h\nu_i < k_BT$. Quantum vibrations do not affect the activation barrier at small driving forces $|\Delta F_0| \ll \lambda$ and the internal reorganization energy originating from quantum vibrations does not need to be accounted for.[35]

While protein powders are indeed nonpolar, surface residues of solvated proteins get ionized and become a significant source of electrostatic fluctuations when moved by low-frequency, elastic fluctuations of the protein shape. Recent measurements have shown that the notion of a nonpolar protein interior is probably far from being correct even for electron transfer in membrane-bound proteins surrounded by a relatively nonpolar lipid medium. For instance, recombination reactions between the quinone cofactors and the P700 radical pair are in the inverted Marcus region with the reorganization energy of ≃0.66 eV at 77 K.[42] Given that this temperature is below the dynamical transition of proteins,[43] one expects a higher reorganization energy at physiological conditions. Consistently with this expectation, a similar reaction within the membrane region between bacteriopheophytin and primary quinone cofactors requires the medium (protein/water/membrane) reorganization energy of ≃1 eV.[44] One has to note that the top of the Marcus parabola, and the corresponding estimate of the reorganization energy, represents the sum of the solvent, λ, and intramolecular, λ_i, reorganization energies even though the reaction rate is not affected by the internal reorganization energy in the normal region when $h\nu_i \gg k_BT$. The reason is that the vibrational Franck−Condon factor is maximized at the vibrational quantum number $n \simeq S$, where $S = \lambda_i/(h\nu_i)$ is the Huang−Rhys factor. The highest reaction rate is then obtained at the driving force equal to $\lambda + h\nu_i S = \lambda + \lambda_i$.

One needs atomistic simulations to estimate the breadth of electrostatic fluctuations produced by the protein-water thermal bath.[45,46] A number of recent MD simulations have reported substantial values of $\lambda \simeq 1.5$ eV, far exceeding the generic estimates from solution studies and in a staggering disagreement with electrochemical measurements. Furthermore, a consistent violation of the prediction of the standard model stipulating $\lambda^{St} = \lambda$ was found in MD simulations of complex membrane-bound protein systems (reaction centers,[45,47] bc_1 complexes,[48,49] and complex I[50]). Specifically, the variance reorganization energy (eq 3) is consistently found to be greater than the Stokes-shift reorganization energy (eq 4)

$$\lambda > \lambda^{St} \tag{5}$$

If one applies the picture of crossing parabolas, the activation barrier is still determined by the Marcus equation (eq 1), but with an effective (reaction) reorganization energy[51,52]

$$\lambda^r = (\lambda^{St})^2/\lambda \tag{6}$$

The basic picture of reorganizing the nuclear degrees of freedom to create the tunneling configuration still applies, but the inequality in eq 5 leads to a lower effective barrier (a protein-induced catalytic effect) consistent with experimental findings.[44,45]

Our simulations of half redox reaction of cytochrome *c* (Cyt-*c*) also produced large values of the reorganization energy, but also showed a much weaker violation of FDR compared to studies of membrane-bound protein complexes:[53] $\lambda^{St} \simeq 1.26 < \lambda \simeq 1.65$ eV. This difference between two reorganization energies was insufficient to produce the experimental[54,55] $\lambda^r \simeq 0.58 \pm 0.04$ eV according to eq 6. It was therefore suggested[53,56] that the polarizability of the active site was the reason for a non-Gaussian statistics[57] of the energy gap X leading to a lower λ^r. Direct simulations incorporating active-site polarizability through the valence-bond formalism[58] supported this conjecture and produced results consistent with existing kinetic data.[56] Uncertainty still exists in whether common nonpolarizable force fields provide a fair estimate of the reorganization parameters provided that they are likely to underestimate the effects of screening of Coulomb interactions by the electronic polarizability.[59]

Given uncertainties in the ability of current force fields to quantitatively describe medium polarization and polarizability of the active site,[60] one needs to study the relatively simple system for which the theory−experiment discrepancy is beyond possible force-field uncertainties. Azurin protein presents such an opportunity (Figure 1). As we show below, simulations of the half reaction with the nonpolarizable active site (point-charge model) produce $\lambda^{St} = 0.96 < \lambda_{Ox} = 1.35 \simeq \lambda_{Red} = 1.44$ eV. These values, when used in eq 6, cannot account for the experimental result $\lambda^r \simeq 0.2-0.3$ eV (Table 1). The discrepancy goes far beyond any possible corrections for screening by the medium-induced dipoles. As we show below, reproducing the experimental results requires assuming that the water component of the reorganization energy is substantially reduced in the configuration of the protein bound to the surface-coated electrode. The statistics of energy gap fluctuations produced by the protein is highly nonergodic, leading to a significant reduction of λ^{St} relative to λ (eq 5).

We start our discussion by analyzing the standard[37] computational algorithm for calculating the electron-transfer activation barrier when the statistics of the electrostatic

https://doi.org/10.1021/acs.jpcb.2c00338
J. Phys. Chem. B 2022, 126, 3000−3011

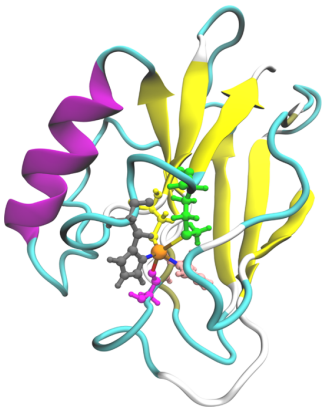

Figure 1. Structure of azurin protein (PDB 1AZU) and its active site. Shown are the Cu atom (orange) and five amino acids ligating it: Gly-45 (magenta), His-46 (pink), Cys-112 (yellow), His-117 (gray), and Met-121 (green). Taken together, they constitute the active site used in quantum calculations (39 heavy atoms for Cu and 5 ligating residues and 77 atoms in the quantum center; 8 hydrogen atoms were added to truncate the broken bonds in the active site).

component of the donor−acceptor energy gap is computed (point-charge model). This is followed by making the active site polarizable and recalculating the statistic of the donor−acceptor energy gap including the free energy of polarizing the active site. We next analyze the effect of altering protonation states of histidines 35 and 83 in azurin (denoted as HSP-35/38 according to CHARMM nomenclature[61]) on the energetics of electron transfer. We finally analyze the statistics of the energy gap from the protein component to show that the experimental λ^{r} falls in between the values obtained for the protein alone and the result of combined protein-water thermal bath. These findings suggest partial desolvation of the protein active site in the process of electrode immobilization of azurin.[62]

PHYSICAL MODEL

The energetics of reduction and oxidation half reactions is controlled by the statistics of the electronic energy level of the molecule in solution relative to the electrochemical potential of the metal electrons μ_m. The energy of the localized electronic state of the reactant fluctuates due to the interaction energy with the medium $\hat{V}_m$ in the system Hamiltonian. For the electron in the ground, reduced (Red) state $|\psi_0\rangle$, the electronic energy affected by the interaction with the medium can be written as the sum of the first- and second-order perturbation terms

$$E = E_0 + \langle\psi_0|\hat{V}_m|\psi_0\rangle - \sum_{k\neq 0}\frac{\langle\psi_0|\hat{V}_m|\psi_k\rangle\langle\psi_k|\hat{V}_m|\psi_0\rangle}{\Delta E_k} \tag{7}$$

where the summation in the last term is over the excited states with the energies E_k separated by the energy gaps $\Delta E_k = E_k - E_0$ from the ground state E_0.

If the charge density of the electron is represented by partial atomic charges (point-charge model), the first-order perturbation term can be viewed as the interaction of atomic charge differences $\Delta q_j = q_j^{Red} - q_j^{Ox}$, representing the distributed charge density of the transferring electron, with the electrostatic potential ϕ_{sj} produced by the medium at the atomic site j

$$\langle\psi_0|\hat{V}_m|\psi_0\rangle = \sum_j \Delta q_j\phi_{sj} \tag{8}$$

where the sum runs over the atomic sites of the quantum center and $\sum_j\Delta q_j = -e$; e is the elementary charge.

The second-order perturbation term describes the polarization of the electronic density by the medium field.[53] It can be written as a tensor contraction of the second-rank tensor of electronic polarizability $\alpha_e(\mathbf{E}_s)$ for the electron at the highest occupied molecular orbital of the Red state with the medium electric field $\mathbf{E}_s$

$$-\sum_{k\neq 0}\frac{\langle\psi_0|\hat{V}_m|\psi_k\rangle\langle\psi_k|\hat{V}_m|\psi_0\rangle}{\Delta E_k} = -\frac{1}{2}\boldsymbol{\alpha}_e(\mathbf{E}_s)\colon \mathbf{E}_s\mathbf{E}_s \tag{9}$$

The polarizability of the electronic state

$$\boldsymbol{\alpha}_e(\mathbf{E}_s) = 2\sum_{k\neq 0}\frac{\mathbf{m}_{0k}\mathbf{m}_{k0}}{\Delta E_k - \Delta\mathbf{m}_k\cdot\mathbf{E}_s} \tag{10}$$

is affected by the medium field through the term in the denominator, which specifies the modulation of the energy gap between the electronically excited and ground states through the interaction of the difference dipole moment $\Delta\mathbf{m}_k = \mathbf{m}_k - \mathbf{m}_0$ with the field; $\mathbf{m}_{0k}$ is the transition dipole between states 0 and k. The polarizability in this form appears from the full valence-bond[58] Hamiltonian matrix of the electronic subsystem when the second-order terms in $\mathbf{m}_{0k}\cdot\mathbf{E}_s$ are collected.[53] With these considerations, the instantaneous, fluctuating energy of the localized electronic state becomes

$$E = E_0 + \sum_j \Delta q_j\phi_{sj} - \frac{1}{2}\boldsymbol{\alpha}_e(\mathbf{E}_s)\colon \mathbf{E}_s\mathbf{E}_s \tag{11}$$

The localized electronic level is lowered with the increase in the local electric field because more free energy is invested in polarizing the solute. This result implies that the redox potential has to decrease when the local field is increased. This was shown to hold by surface-enhanced resonance Raman spectroscopy of tetraheme cytochromes immobilized on self-assembled monolayers (SAMs).[63]

Electronic transitions effectively occur from (reduction) and to (oxidation) the highest occupied electronic level in the metal with the electrochemical potential μ_m in the Marcus−Levich[64−66] description of nonadiabatic electrode reactions. The energy−gap reaction coordinate[37] for an electrode reaction becomes (Figure 2)

$$X = E - \mu_m = E_0 - \mu_m + X^C_{pol} \tag{12}$$

where

$$X^C_{pol} = X^C - \frac{1}{2}\boldsymbol{\alpha}_e(\mathbf{E}_s)\colon \mathbf{E}_s\mathbf{E}_s \tag{13}$$

and

$$X^C = \sum_j \Delta q_j\phi_{sj} \tag{14}$$

is the Coulomb component of the energy gap.

The standard formulation of nonadiabatic reaction rates[65,66] leads to the redox rate constant proportional to the Gaussian probability (eq 2) of reaching zero energy gap $X = 0$. The condition of equal rates at equilibrium defines the stationary electrochemical potential μ_m^{eq} as

https://doi.org/10.1021/acs.jpcb.2c00338
J. Phys. Chem. B 2022, 126, 3000−3011

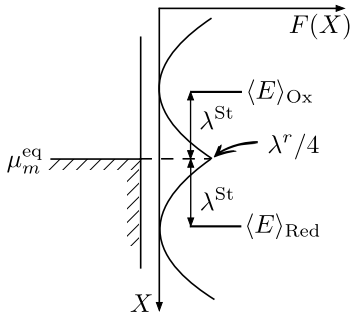

Figure 2. Schematics of the energy levels and the energy-gap reaction coordinate in the electrode half reaction of electron transfer. The crossing parabolas represent the free energy surface $F(X)$ of electron transfer vs the energy-gap reaction coordinate X. The configuration of energy levels shown here corresponds to the equilibrium electrode potential μ_m^{eq} (eq 15) when rates of oxidation and reduction are equal and there is no driving force for an electrode half reaction.

$$\mu_m^{eq} = \frac{1}{2}[\langle E\rangle_{Ox} + \langle E\rangle_{Red}] \tag{15}$$

where the angular brackets $\langle ...\rangle_{Ox,Red}$ specify the statistical averages in the corresponding oxidation state. The instantaneous value of the reaction coordinate becomes

$$X = \lambda^{St} + \delta X^{C}_{pol} \tag{16}$$

where $\delta(...)$ denotes the deviation from the average values in the Ox state and, for the half reaction (cf. to eq 4), one obtains

$$\lambda^{St} = \frac{1}{2}[\langle E\rangle_{Ox} - \langle E\rangle_{Red}] \tag{17}$$

With this definition, the standard electrode rate constant based on the average energy gap and the gap variance in the Gaussian probability (eq 2) becomes

$$k_0 \propto \exp\left[-\frac{(\lambda^{St})^2}{2\sigma_X^2}\right] = \exp\left[-\beta\frac{\lambda^r}{4}\right] \tag{18}$$

where $\beta = (k_B T)^{-1}$ is the inverse temperature. Equations 17 and 18 state that the average energy separation between the oxidized state and the electrochemical potential of the metal is given by λ^{St} (Figure 2) and the variance of fluctuations around the average is specified by λ (eq 3). When summation over the Fermi distribution of the electronic energy level in the metal is included in the rate calculation, one obtains a somewhat more accurate expression[66]

$$k_0 \propto \mathrm{erfc}(\sqrt{\beta\lambda^r}/2) \tag{19}$$

where $\mathrm{erfc}(x)$ is the complementary error function. Equations 16 and 18 imply that no driving force is required to describe forward and backward standard reaction rates at the equilibrium electrode potential. The continuously changing electrode overpotential η, $-e\eta = \mu_m - \mu_m^{eq}$ plays the role of the electron-transfer driving force $\Delta F_0 = e\eta$ in the electrochemical experiment.[67] The reorganization energy of a protein half reaction can be extracted,[68,69] for instance, from the "trumpet plot" displaying the oxidation and reduction peak potentials in cyclic voltammetry versus the logarithm of the scan rate.[56,70]

Nonergodic Statistics of Protein Fluctuations. The Gaussian statistics of the energy-gap reaction coordinate is used in the derivation outlined in the Introduction and detailed here for an electrode half reaction. Polar liquids considered as thermal bath in the Marcus theory possess sufficient fluidity to fully adjust to changing electrostatics of the transferring electron. The lack of flexibility and frustration of a folded protein do not allow such complete adjustment. Therefore, average energy gaps $\langle X\rangle_i$ in two electron-transfer configurations represent structures that are incompletely relaxed in terms of electrostatics (Figure 3) as signaled by the presence of

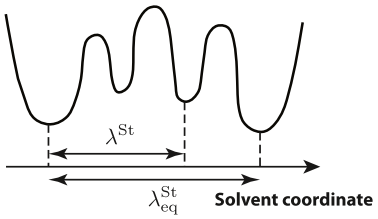

Figure 3. Illustration of the reduced separation between the average energy gaps $\langle X\rangle_i$ (i = Ox, Red) in the frustrated protein medium not allowing full equilibration with the electric field of the transferring electron. The wiggled line is a schematic projection of the full energy landscape of the protein on a small subset of degrees of freedom of protein and water ("solvent coordinate") coupled to electron transfer. The one-dimensional representation is an illustration of a multidimensional partial free energy surface (i.e., the potential of mean force) serving as the vertical axis.

an unrelaxed electric field inside the protein[71] and the corresponding electrostatic stress[72] (see the discussion of the electric field in the active site below). Note that a minimum corresponding to the configuration fully relaxed to the electrostatic perturbation might not even exist if it comes in conflict with the structural stability of the folded protein. The difference of average energy gaps $\langle X\rangle_i$, representing some intermediate local minima on the energy landscape of the protein (Figure 3), does not connect in this scenario to the equilibrium, thermodynamic Marcus reorganization energy and one arrives at the inequality between λ^{St} and λ (eq 5). Two unequal reorganization energies combine in the reduced reaction reorganization energy λ^r (eq 6) recorded by kinetic measurements.

Nonergodic sampling of statistical configurations leading to eq 5 can be achieved by a number of mechanisms. Protonation/deprotonation equilibria are one of them. Measurements of the protein charge by protein charge ladders[73] analyzed with capillary electrophoresis have shown that azurin's charge changes by -0.51 ± 0.04 units of elementary charge upon electron transfer.[74] The fractional charge is assigned to changes in the protonation state of non-coordinating residues, predominantly histidines (His). According to FDR argument, the response is equivalent to fluctuations: changes in the protonation state upon altering charge must reflect fluctuations of proton binding coupled to charge transfer. This observation poses the question of whether ionizable protons should be included in the list of nuclear degrees of freedom that reorganize to drive protein electron transfer. The answer depends on the relative magnitudes of the reaction rate and the rate of protonation/deprotonation.

If protonation/deprotonation of amino acids were fast compared to the reaction time for oxidation/reduction, one would obtain many proton exchange events on the reaction time $\tau_{ET} \simeq k_{ET}^{-1}$ and could apply Gibbsian statistics[75] to the statistical average. These exchange events involve single

https://doi.org/10.1021/acs.jpcb.2c00338
J. Phys. Chem. B 2022, 126, 3000−3011

particles and produce non-Gaussian telegraphic noise.[76,77] Deviations from the Gaussian picture of crossing parabolas follow, also for wetting by hydration water involving only a few molecules.[78] However, protonation/deprotonation reactions are typically slow and essentially no such events occur on the reaction time τ_{ET}. This is the limit of extreme nonergodicity, similar to the well-established Franck−Condon principle in molecular spectroscopy. No protonation/deprotonation transitions occur on the reaction time scale, but these events happen before and after electron transfer and can be accomplished during a much longer waiting time before the next reaction event. Therefore, such slow protonation/deprotonation equilibria contribute only to heterogeneous population kinetics and do not affect the electron-transfer rate constant calculated for a specific protonation configuration.

To evaluate the effect of protonation/deprotonation equilibria on the reaction kinetics, consider the protonation of a residue located at the distance r from the active site. The electronic energy of the active site $\tilde{E}$ in the protein in the protonated state is related to the active-site energy E in the deprotonated state as

$$\tilde{E} = E - \frac{e^2}{\epsilon_{eff} r} \tag{20}$$

where ϵ_{eff} is the effective dielectric constant of the screening medium. If the energy alteration happens sufficiently fast, on the time scale shorter than τ_{ET}, many random fluctuations between E and $\tilde{E}$ will contribute to the Gaussian variance σ_X and the average $\langle X \rangle_i$. Alternatively, one has to assign individual rates to each protonation state and take a weighted average in the decay of populations for Ox or Red states.

■ ENERGETICS OF ELECTRON TRANSFER

Polarizability of the Active Site. Blue copper proteins are well known for their bright colors deriving from the ligand-to-metal charge-transfer transitions.[39,79] The intense optical transition ($\epsilon \sim 500$ M^{-1} cm^{-1}) in azurin's oxidized state is enabled by the covalent character of the Cu−S(Cys-112) bond in the active site. Absorption of light leads to charge transfer[79] from the pπ orbital of S(Cys-112) to the $3d_{x^2-y^2}$ half-occupied orbital of Cu^{II}. The optical transition is associated with the transition dipole $M_{CT} \simeq 4.4$ D, the absorption frequency $\hbar\omega_{abs} \simeq 2$ eV[80] and the corresponding polarizability

$$\alpha_{CT}^{xx} = 2\frac{M_{CT}^2}{\hbar\omega_{abs}} \simeq 31.6 \text{ Å}^3 \tag{21}$$

where the x-axis of the body frame is chosen along the Cu−S(Cys-112) bond. The charge-transfer absorption band involves three Gaussian sub-bands, and the full fit yields $\alpha_{CT} = 44.6$ Å^3 (see the Supporting Information). The reduced azurin has a $3d^{10}$ electronic configuration and shows much reduced absorption intensity. The polarizability of the highest occupied level in the Ox state of the active site (eq 10) was calculated with ZINDO and CIS/3-21* methods involving 1000 and 500 excited states, respectively (see the Supporting Information). The value $\alpha_e \simeq 12-14$ Å^3 falls below the spectroscopic result by a factor of ≃3, thus confirming the general trend of quantum calculations to underestimate the molecular polarizability.[81] Based on spectroscopic evidence, we anticipate that the active site must be more polarizable than what follows from the present quantum calculations.

The vacuum polarizability tensor α_e in the body frame of the active site is anisotropic (Red state, ZINDO calculation, Å^3)

$$\boldsymbol{\alpha}_e = \begin{pmatrix} 18.20 & 1.78 & 0.48 \\ 1.78 & 15.97 & 1.25 \\ 0.48 & 1.25 & 14.13 \end{pmatrix} \tag{22}$$

The largest (α_e^{xx}) component is along the Cu−S(Cys-112) bond. We also find that the electric field of the protein-water thermal bath at the active site is highly anisotropic, with a large average value, $\langle E_{sx} \rangle \simeq 0.4$ V/Å, also along the Cu−S(Cys-112) bond (Figure 4). The active site is, therefore, oriented within

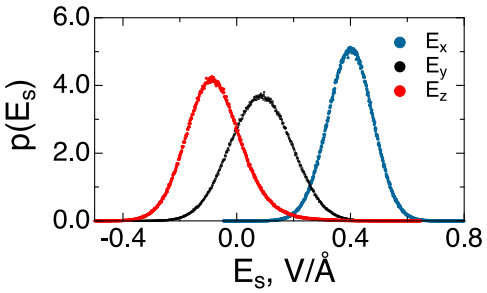

Figure 4. Normalized distributions of the electric field from the protein-water thermal bath at the azurin active site calculated in the body frame of the protein. The x-axis of the body frame is along the Cu−S(Cys-112) bond, the y-axis is in the plane of (protein center of mass)-Cu−S(Cys-112) points, and the z-axis is perpendicular to this plane.

the protein scaffold to allow the strongest coupling of the electronic polarizability with the medium field. A very similar situation was found for the heme of Cyt-c.[60] However, with our current polarizability calculations, the effect of field anisotropy on the distribution of the electron-transfer energy gap is less significant for azurin than for Cyt-c.

The normalized distributions of the Coulomb energy gap X^C (eq 14) for the Red and Ox states are shown in Figure 5. They are compared to distributions of the energy gap X_{pol}^C (eq 13) including the free energy of polarizing the active site. The resulting reorganization energies λ^{St} and λ are listed in Table 2.

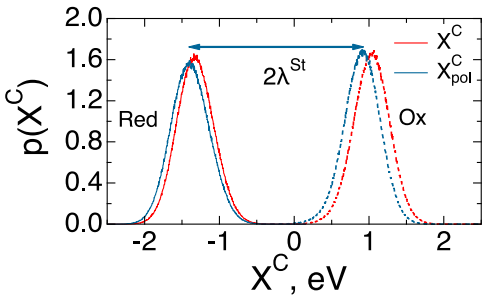

Figure 5. Normalized distributions of the Coulomb component of the energy gap in Red and Ox states of azurin. The red lines indicate the distributions of the Coulomb energy X^C due to atomic charges Δq_j at the active site (eq 14). The blue lines show the distribution of energies X_{pol}^C including the free energy of polarizing the electronic density of the active site (eq 13). The separation between the distribution maxima $2\lambda^{St}$ specifies the Stokes-shift reorganization energy, the distribution width provides the reorganization energy λ.

https://doi.org/10.1021/acs.jpcb.2c00338
J. Phys. Chem. B 2022, 126, 3000−3011

Table 2. Reorganization Energies[a] of Azurin (eV)

		nonpolarizable					polarizable				
state	Q	λ_L^{St}	λ_L	λ^{St}	λ	λ^r	λ_L^{St}	λ_L	λ^{St}	λ	λ^r
Red	−3	1.17	1.17	0.99	1.36	0.72	1.15	1.25	0.96	1.44	0.66
Ox	−2		1.16		1.35			1.16		1.35	
Ox/HSP-35[b]	−1	1.03	0.92	0.85	1.11	0.58	1.04	0.90	0.85	1.08	0.57
Ox/HSP-83	−1	1.06	1.01	0.87	1.20	0.59	1.05	0.99	0.86	1.18	0.57
Ox/HSP-35/83	0	1.03	0.94	0.84	1.13	0.57	1.03	0.91	0.84	1.09	0.56

[a]The reaction reorganization energy λ^r is calculated from eq 6 by taking the variance reorganization energy as the average of Ox and Red values $\lambda = (\lambda_{Ox} + \lambda_{Red})/2$. [b]HSP-35 and HSP-83 refer to azurin mutants with a single protonates histidine residue; HSP-35/83 is the mutant with both histidines in the protonated state.

In addition to the apparent reorganization parameters obtained directly from simulations and specified with the subscript "L" (referring to the size L of the cubic simulation box), Table 2 lists the reorganization energies corrected for finite size effects (with the subscript dropped).

The simulation protocol used to produce finite-size reorganization energies listed in Table 2 is described in detail in the Supporting Information. Briefly, following our previously established protocols,[53,56,60,78] MD simulations of azurin (PDB code 1AZU) hydrated with 36469 TIP3P water molecules were performed using NAMD simulation software.[82] Production NVT trajectories were accumulated for 300 ns for each redox and protonation state. The difference charges Δq_j in eq 14 required for the Coulomb component of the electron-transfer energy gap were calculated from DFT/B3LYP/6-31g(d,p) in different schemes for extracting the atomic charges (Tables S5−S12). The CHELPG scheme for Δq_j was adopted.

The reorganization energies for half redox reactions are noticeably affected by finite size effects as was first shown by Ayala and Sprik.[83] The need for such corrections comes from the fact that changing the oxidation state in a half reaction makes the overall charge of the simulation cell nonzero. This difficulty, which also appears in simulations of ionic solvation,[84] is the result of the Coulomb interaction of the transferring charge with the uniform charge background of the simulation cell in the Ewald-sum protocol.[85] It appears[86] that the finite-size correction term enters λ_L^{St} and λ_L with opposite signs

$$\lambda = \lambda_L - \frac{1}{2}e^2(1-\epsilon^{-1})\bar{\zeta}$$
$$\lambda^{St} = \lambda_L^{St} + \frac{1}{2}e^2(1-\epsilon^{-1})\bar{\zeta} \quad (23)$$

The formula for $\bar{\zeta}$ in this equation was derived by Hünenberger and McCammon[87,88]

$$\bar{\zeta}(R, L) = \xi + \frac{\Omega}{RL^3} - \frac{\Omega^2}{5RL^6} \quad (24)$$

for a spherical solute with the radius R and volume $\Omega = (4\pi/3)R^3$ placed in the cubic simulation cell with the side length L; $\xi = -2.837298/L$ is the Wigner potential of the lattice of replicas of the central cell surrounded by a conducting sphere[89] and ϵ is the dielectric constant of the medium ($\epsilon \simeq 91$ for TIP3P water at 298 K used in simulations). Adding/subtracting the finite-size correction term makes λ about 10% higher than λ_L and λ^{St} lower than λ_L^{St} by the same amount. In short, finite-size corrections separate λ^{St} and λ by about 20% of their apparent values obtained from simulations (Table 2).

We also notice that the polarizability of the active site $\boldsymbol{\alpha}_e(\mathbf{E}_s)$ is modulated by fluctuations of the electric field coupled to the dipole moment differences $\Delta\mathbf{m}_{0k}$ in eq 10. The distributions of polarizability traces $\alpha_e = (1/3)\mathrm{Tr}[\boldsymbol{\alpha}_e(\mathbf{E}_s)]$ calculated on trajectories for Ox and Red states are shown in Figure 6.

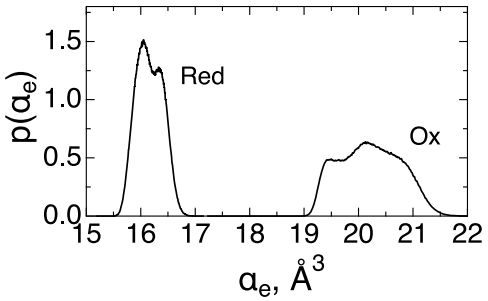

Figure 6. Normalized distributions of the polarizability trace $\alpha_e = (1/3)\mathrm{Tr}[\boldsymbol{\alpha}_e(\mathbf{E}_s)]$ referring to the highest occupied electronic state of the active site calculated from eq 10 and MD trajectories of the electric field in the Ox and Red states of azurin.

Overall, the effect of polarizability on the reorganization energies is modest in the present calculations. This comes in contrast to strong polarizability effects found for Cyt-c[53,60] where strongly anisotropic, and higher in magnitude, polarizability of the heme combines with a matching anisotropy of the electric field of the protein-water medium to produce a significant separation of the Stokes-shift and variance reorganization energies (eq 5). Similar matching anisotropies between the active-site polarizability and the medium field are found here for azurin where the direction of the Cu−S bond displaying charge-transfer character[39] shows both the highest polarizability and the highest medium field. Given that our quantum calculations fail to reproduce a large transition dipole of the charge-transfer optical transition responsible for the bright color of Ox azurin, our calculations are likely to underestimate both the polarizability magnitude and its anisotropy. Therefore, the separation between λ^{St} and λ reported here will increase when more realistic polarizability estimates become available. Note that a full description of the effect of polarizability on electron transfer requires globally nonparabolic free energy surfaces,[57] and our reliance here on the picture of crossing parabolas[2] serves as a simple, even though not exact, mathematical route to the activation barrier. It also appears that partial desolvation[63] of the protein in electrochemical interfacial experiments provides a more robust explanation for the low electrochemical values of λ^r listed in Table 1.

https://doi.org/10.1021/acs.jpcb.2c00338
J. Phys. Chem. B 2022, 126, 3000−3011

Table 3. Protein Reorganization Energies (eV)

		nonpolarizable					polarizable				
State	Q	λ_L^{St}	λ_L	λ^{St}	λ	λ^r	λ_L^{St}	λ_L	λ^{St}	λ	λ^r
					Azurin						
Red	−3	0.50	1.31	0.31	1.49	0.06	0.47	1.35	0.28	1.54	0.05
Ox	−2		1.51		1.70			1.52		1.71	
					Cyt-c^a						
Red	8	0.68	2.97	0.88	3.16	0.27					
Ox	9		2.28		2.47	(0.22^b)					

[a]Simulation trajectories from ref 53 in the point-charge model of the active site. [b]Experimental value for Cyt-*c* electrostatically attached to the SAM.[91]

Reorganization of the Protein. The conditions of electrochemical experiment, where the protein is immobilized on the SAM coating the metal electrode, can be substantially distinct from the solution simulations carried out here.[62,90] The hydration shell around the active site is grossly reduced by attachment, and fluctuations of the protein might become the leading component of the entire fluctuation spectrum of the thermal bath. Furthermore, from the fundamental perspective, it is the frustrated protein scaffold that is expected to demonstrate nonergodic statistics of electrostatic fluctuations and one wants to know the extent of separation between λ^{St} and λ for the protein component alone. These results are listed in Table 3 (Q is the protein charge). The free energy surfaces of electron transfer[57]

$$F(X) = -\beta^{-1} \ln[p(X)] \tag{25}$$

[$p(X)$ is the normalized probability density, Figure 5] from the protein alone are compared to the entire protein-water system in Figure 7.

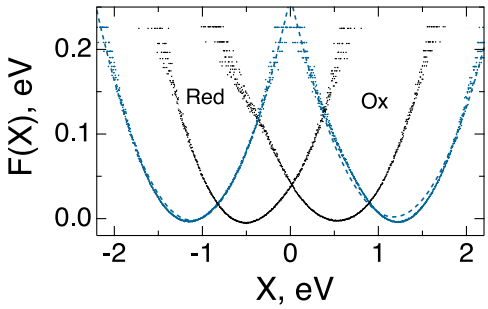

Figure 7. Free energy surfaces $F(X)$ (eq 25) for the half reaction of electron transfer from metal to azurin (Ox) and from azurin (Red) to the metal electrode at the equilibrium electrode potential (eq 15). The values of X from simulations are shifted to ensure the crossing of the free energy surfaces at $X = 0$ of electron transfer to/from the highest occupied electronic state in the metal with the electrochemical potential μ_m^{eq} (Figure 2). The blue points refer to the entire protein-water thermal bath, while the black points refer to the protein only. The dashed lines are parabolic fits of the free energy surfaces calculated from simulations.

Thermal fluctuations of the protein display a significant extent of nonergodicity, with the ratio of reorganization energies $\lambda/\lambda^{St} \simeq 6$ for azurin. Such a large distinction between the Stokes-shift and variance reorganization energies leads to the kinetic reorganization energy λ^r significantly below experimental observations (Tables 1 and 3). Comparison between λ^r values obtained from full solution simulations (Table 2) to the protein reorganization energies (Table 3) allows us to suggest that azurin is partially desolvated when attached to the SAM, with λ^r falling in between the all-solvated and protein-only values.

Similar phenomenology applies to Cyt-*c* with $\lambda/\lambda^{St} \simeq 3.6$ for the protein component (Table 3). The results of electrochemical kinetic measurements were supported by the model involving a polarizable heme. The corresponding experimental data were obtained for Cyt-*c* proteins immobilized by linking the heme to the terminal pyridine group of the PyC_{11}/C_{10} monolayer.[70,92] On the other hand, electrostatic immobilization of Cyt-*c* significantly lowers the observed reorganization energy to ≃0.22 eV, which is expected to predominantly arise from the protein polarization.[91] This outcome is indeed consistent with the number for Cyt-*c* listed in Table 3. In contrast to Cyt-*c*, immobilization of azurin is achieved through hydrophobic interactions between the hydrophobic area around the copper atom and methyl heads of alkanethiol.[9,93] The binding site of azurin is a largely hydrophobic domain that includes the nitrogen (NE2) atom of the partially solvent exposed copper ligand His-117.[11] Immobilization of Cyt-*c* and azurin is thus achieved through different binding motifs. Investigation of electrochemical kinetics on methyl- and OH-terminated SAMs has shown about 20% higher reorganization energies for hydrophilic surfaces compared to hydrophobic SAMs.[11] This reproducible change suggests a larger solvent contribution to reorganization energy for hydrophilic binding as ascribed to enhanced water accessibility to the protein metal center. All these experimental observations support the assessment that low values of λ^r should be ascribed to protein reorganization, which becomes the dominant component of the activation barrier for partially desolvated metalloproteins adsorbed either to SAMs in electrochemical experiments or to large protein complexes in biological energy chains.

Altering Protonation State. Altering protonation state of histidine (His-35 and His-83) residues in azurin can affect electrostatics of the active site (eq 20) and the activation barrier of electron transfer. Conversion between protonated and deprotonated forms was reported for His-35[94] in the pH range ≃ 4.9−8.5 of the titration curve. In contrast, His-83 with[8] $pK_{red} = 7.72$ and $pK_{ox} = 7.50$ is often viewed as protonated in both oxidation states of azurin. To study the effect of altering electrostatics on the half reaction of electron transfer, simulations of three mutants with protonated histidines were done in the Ox state of the active site (Table 2). The average distances between the Cu atom and the protonation sites of histidines from MD simulations are 7.71 Å (His-35) and 14.62 Å (His-83). The corresponding shifts of $\langle X^C \rangle$ compared to the corresponding deprotonated Ox state are −0.27, −0.22, and −0.28 eV. The last value refers to the

https://doi.org/10.1021/acs.jpcb.2c00338
J. Phys. Chem. B 2022, 126, 3000−3011

double protonated Ox state (HSP-35/83 in Table 2). Based on eq 20, the first two shifts require $\epsilon_{\text{eff}} \simeq 4.5-7$ for the protein dielectric screening medium.

The reorganization parameters listed in Table 2 are for a hypothetical electronic transition from the deprotonated Red state to three different protonated Ox states. This condition corresponds to nonergodic protonation, which is slower than the electron-transfer reaction, thus leading to several distinct rate constants. If one alternatively assumes ergodic protonation, then switching between different protonation states should lead to a telegraphic electrostatic noise broadening the distribution of electron-transfer energy gaps. Such a combined trajectory can be produced by a Monte Carlo formalism switching between different trajectories corresponding to each protonation state. One might anticipate that the highest extent of broadening is achieved when all states are equally populated. Such simulations produce a relatively small extent of broadening of the energy gap distribution shifting the variance reorganization energy from $\lambda \simeq 1.16$ eV for a deprotonated Ox state (nonpolarizable model) to $\lambda \simeq 1.26$ eV when all three protonation states equally contribute to the gap distribution. We can conclude that even the fully ergodic configuration of fast protonation−deprotonation of histidine residues does not strongly affect the statistics of the energy gap. Protonation equilibria of far-away residues, which are not in direct electrostatic contact with the active site, do not significantly affect the kinetics of electron transfer (Figure 8).

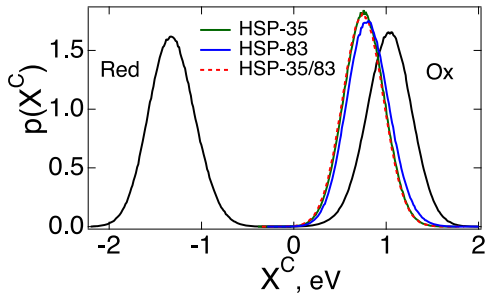

Figure 8. Normalized distributions of the Coulomb component of the energy gap in Red and Ox states of azurin. The Ox state includes different protonation states of His-35 and His-83 residues; HSP-35 and HSP-83 specify states with a single protonated residue and HSP-35/83 refers to the state in which both His residues are protonated.

DISCUSSION

We have considered several physical mechanisms to explain small activation barriers for electrochemical kinetics of azurin (Table 1): (1) electronic polarizability of the active site, (2) altering protonation states of far-away histidine residues not directly connected to the active site, and (3) partial desolvation of the protein when attached to the surface monolayer. Based on the active sites polarizability from quantum calculations and separate simulations of protonated states of His-35 and His-83 residues, the first two mechanisms do not provide sufficient lowering of the activation barrier. There are good indications that the active site polarizability is significantly underestimated by the present quantum calculations and smaller activation barriers are anticipated for more polarizable active sites. The calculations result in the reaction (kinetic) reorganization energy $\lambda^{\text{r}} \simeq 0.66$ eV (Table 2), which is close in magnitude to $\lambda^{\text{r}} \simeq 0.57$ eV found in previous calculations for Cyt-*c* involving a polarizable active site.[56] Nevertheless, this value still significantly exceeds $\lambda^{\text{r}} \simeq 0.2-0.3$ eV reported by electrochemical kinetic measurements (Table 1). The last mechanism, partial protein desolvation, seems to deliver the most robust explanation of experimental findings. The reorganization energies λ^{St} and λ are strongly separated for the protein component of the thermal bath (Table 3). Elimination of the water layer when the protein is attached to the SAM-coated electrode is the main reason for the low activation barrier.

The suggested mechanism is consistent with a number of previous observations that large membrane-bound protein complexes[45,48−50] demonstrate most significant violation of FDRs. It is the constrained and frustrated protein scaffold that allows $\lambda^{\text{St}} < \lambda$. The water shell around a small soluble protein substantially balances this effect out. Hence, the protein complex has to be large to shield water out and to allow nonergodic protein electron transfer, or, alternatively, the water shell needs to be pushed away for an interfacial reaction.

All mechanisms considered here require significant departure from the standard Marcus theory of electron transfer, which was developed for homogeneous polar liquids producing Gaussian fluctuations of the localized electronic states subject to FDR constraints. Application of these ideas to protein electron transfer raises the question of how far the underlying assumptions can still be applied to the heterogeneous protein-water thermal bath as opposed to the homogeneous polar liquid considered in the Marcus theory.

From the general perspective, electrostatic coupling between the transferring electron and the medium involves many particles of the medium and thus puts the problem under the umbrella of the central limit theorem. The energy gap fluctuations are mostly Gaussian, masking many of the potential difficulties with other assumptions of the model. The FDR requires λ^{St} and λ to be equal and the variance of the energy gap to scale linearly with the temperature $\sigma_X^2 \propto T$ (eq 3). It thus describes the shift of the medium to a new equilibrium, under an external force, while preserving the medium structure (in analogy to a spring stretching in response to an external force, but not changing its force constant). If the structure of the medium is altered, the FDRs must be violated. Changes of the protein structure, or of its protonation state, must lead to various levels of departure from the standard Marcus theory, which is based on the validity of FDRs.

In addition to these considerations, the protein fold imposes severe restrictions on the ability of the medium to fully equilibrate with a given electronic state. These restrictions can be either structural, implying that full equilibration cannot be reached, or dynamic, meaning that such equilibration might require times longer than the reaction time. In the former case, mechanical equilibrium is reached without ever attaining the electrostatic equilibrium. In the latter case, the full ensemble of configurations is not accessible on the reaction time and the ensemble of configurations is nonergodic. The structural recovery time can be 2−3 times longer than α-relaxation described by FDRs in simple liquids,[95] but can take even longer time for proteins. The mechanistic consequence of these various mechanisms is reflected in a separation between λ^{St} and λ. Because only two moments of the energy gap are meaningful in the Gaussian statistics, all the complexity of the protein-water thermal bath is hidden in this fairly simple phenomenology.

https://doi.org/10.1021/acs.jpcb.2c00338
J. Phys. Chem. B 2022, 126, 3000−3011

The effect of the oxidation state on pK_a values of ionizable residues and their electrostatic effect on the reaction kinetics provide a potential mechanism for allostery when changing the oxidation state on one site can trigger the corresponding redox reaction on a distant site. This electrostatically driven allostery becomes an alternative to the usually anticipated elastic allostery driven by conformational transitions. However, our present calculations do not support this attractive hypothesis: the electrostatic coupling of far-away ionizable residues to the active site turns out to be insufficient to noticeably affect a redox reaction. In addition, changing the ionization state must be a process sufficiently fast on the reaction time scale. When this does not happen and altering ionization state is a nonergodic process, the electrostatic coupling provides a constant shift of the energy gap, which cancels out in either Stokes or variance reorganization energies fully specifying the activation barrier.

■ ASSOCIATED CONTENT

Supporting Information

The Supporting Information is available free of charge at https://pubs.acs.org/doi/10.1021/acs.jpcb.2c00338.

Protocols of MD simulations, details of quantum calculations, and additional results of the theoretical analysis and experimental data (PDF)

■ AUTHOR INFORMATION

Corresponding Author

Dmitry V. Matyushov − *School of Molecular Sciences and Department of Physics, Arizona State University, Tempe, Arizona 85287-1504, United States;* orcid.org/0000-0002-9352-764X; Email: dmitrym@asu.edu

Author

Setare M. Sarhangi − *Department of Physics, Arizona State University, Tempe, Arizona 85287-1504, United States*

Complete contact information is available at: https://pubs.acs.org/10.1021/acs.jpcb.2c00338

Notes

The authors declare no competing financial interest.

■ ACKNOWLEDGMENTS

This research was supported by the National Science Foundation (CHE-2154465) and by the Army Research Office (ARO-W911NF2010320).

■ REFERENCES

(1) Nicholls, D. G.; Ferguson, S. J. *Bioenergetics*, 4th ed.; Academic Press: Amsterdam, 2013.

(2) Marcus, R. A.; Sutin, N. Electron transfers in chemistry and biology. *Biochim. Biophys. Acta* **1985**, *811*, 265−322.

(3) Page, C. C.; Moser, C. C.; Chen, X.; Dutton, P. L. Natural engineering principles of electron tunnelling in biological oxidation-reduction. *Nature* **1999**, *402*, 47−52.

(4) Gray, H. B.; Winkler, J. R. Long-range electron transfer. *Proc. Natl. Acad. Sci. U.S.A.* **2005**, *102*, 3534−3539.

(5) Gray, H. B.; Winkler, J. R. Electron tunneling through proteins. *Q. Rev. Biophys.* **2003**, *36*, 341−372.

(6) Farver, O.; Hosseinzadeh, P.; Marshall, N. M.; Wherland, S.; Lu, Y.; Pecht, I. Long-range electron transfer in engineered azurins exhibits Marcus inverted region behavior. *J. Phys. Chem. Lett.* **2014**, *6*, 100−105.

(7) Chi, Q.; Farver, O.; Ulstrup, J. Long-range protein electron transfer observed at the single-molecule level: In situ mapping of redox-gated tunneling resonance. *Proc. Natl. Acad. Sci. U.S.A.* **2005**, *102*, 16203−16208.

(8) Guo, Y.; Zhao, J.; Yin, X.; Gao, X.; Tian, Y. Electrochemistry Investigation on Protein Protection by Alkanethiol Self-Assembled Monolayers against Urea Impact. *J. Phys. Chem. C* **2008**, *112*, 6013−6021.

(9) Khoshtariya, D. E.; Dolidze, T. D.; Shushanyan, M.; Davis, K. L.; Waldeck, D. H.; van Eldik, R. Fundamental signatures of short- and long-range electron transfer for the blue copper protein azurin at Au/SAM junctions. *Proc. Natl. Acad. Sci. U.S.A.* **2010**, *107*, 2757−2762.

(10) Monari, S.; Battistuzzi, G.; Bortolotti, C. A.; Yanagisawa, S.; Sato, K.; Li, C.; Salard, I.; Kostrz, D.; Borsari, M.; Ranieri, A.; et al. Understanding the mechanism of short-range electron transfer using an immobilized cupredoxin. *J. Am. Chem. Soc.* **2012**, *134*, 11848−11851.

(11) Zitare, U. A.; Szuster, J.; Santalla, M. C.; Morgada, M. N.; Vila, A. J.; Murgida, D. H. Dynamical effects in metalloprotein heterogeneous electron transfer. *Electrochim. Acta* **2020**, *342*, 136095.

(12) Blumberger, J. Free energies for biological electron transfer from QM/MM calculation: method, application and critical assessment. *Phys. Chem. Chem. Phys.* **2008**, *10*, 5651−5667.

(13) Alessandrini, A.; Corni, S.; Facci, P. Unravelling single metalloprotein electron transfer by scanning probe techniques. *Phys. Chem. Chem. Phys.* **2006**, *8*, 4383−4397.

(14) Paltrinieri, L.; Borsari, M.; Ranieri, A.; Battistuzzi, G.; Corni, S.; Bortolotti, C. A. The active site loop modulates the reorganization energy of blue copper proteins by controlling the dynamic interplay with solvent. *J. Phys. Chem. Lett.* **2013**, *4*, 710−715.

(15) Shen, L.; Zeng, X.; Hu, H.; Hu, X.; Yang, W. Accurate quantum mechanical/molecular mechanical calculations of reduction potentials in azurin variants. *J. Chem. Theory Comput.* **2018**, *14*, 4948−4957.

(16) Jin, H.; Goyal, P.; Das, A. K.; Gaus, M.; Meuwly, M.; Cui, Q. Copper oxidation/reduction in water and protein: Studies with DFTB3/MM and VALBOND molecular dynamics simulations. *J. Phys. Chem. B* **2015**, *120*, 1894−1910.

(17) Warshel, A.; Sharma, P. K.; Kato, M.; Xiang, Y.; Liu, H.; Olsson, M. H. M. Electrostatic basis for enzyme catalysis. *Chem. Rev.* **2006**, *106*, 3210−3235.

(18) Nar, H.; Messerschmidt, A.; Huber, R.; van de Kamp, M.; Canters, G. W. Crystal structure analysis of oxidized Pseudomonas aeruginosa azurin at pH 5·5 and pH 9·0. *J. Mol. Biol.* **1991**, *221*, 765−772.

(19) Frauenfelder, H.; Chen, G.; Berendzen, J.; Fenimore, P. W.; Jansson, H.; McMahon, B. H.; Stroe, I. R.; Swenson, J.; Young, R. D. A unified model of protein dynamics. *Proc. Natl. Acad. Sci. U.S.A.* **2009**, *106*, 5129−5134.

(20) Frauenfelder, H. In *The Physics of Proteins. An Introduction to Biological Physics and Molecular Biophysics*; Chan, S. S., Chan, W. S., Eds.; Springer: New York, 2010.

(21) McMahon, B. H.; Müller, J. D.; Wraight, C. A.; Nienhaus, G. U. Electron transfer and protein dynamics in the photosynthetic reaction center. *Biophys. J.* **1998**, *74*, 2567−2587.

(22) Yang, H.; Luo, G.; Karnchanaphanurach, P.; Louie, T.-M.; Rech, I.; Cova, S.; Xun, L.; Xie, X. S. Protein conformational dynamics probed by single-molecule electron transfer. *Science* **2003**, *302*, 262−266.

(23) Pudney, C. R.; Lane, R. S. K.; Fielding, A. J.; Magennis, S. W.; Hay, S.; Scrutton, N. S. Enzymatic single-molecule kinetic isotope effects. *J. Am. Chem. Soc.* **2013**, *135*, 3855−3864.

(24) Gupta, A.; Aartsma, T. J.; Canters, G. W. One at a time: Intramolecular electron-transfer kinetics in small laccase observed during turnover. *J. Am. Chem. Soc.* **2014**, *136*, 2707−2710.

(25) Pradhan, B.; Engelhard, C.; Van Mulken, S.; Miao, X.; Canters, G. W.; Orrit, M. Single electron transfer events and dynamical heterogeneity in the small protein azurin from Pseudomonas aeruginosa. *Chem. Sci.* **2019**, *11*, 763−771.

(26) Brujić, J.; Hermans Z, R. I.; Walther, K. A.; Fernandez, J. M. Single-molecule force spectroscopy reveals signatures of glassy dynamics in the energy landscape of ubiquitin. *Nat. Phys.* **2006**, *2*, 282−286.
(27) Xie, X. S. Enzyme kinetics, past and present. *Science* **2013**, *342*, 1457−1459.
(28) Engelkamp, H.; Hatzakis, N. S.; Hofkens, J.; De Schryver, F. C.; Nolte, R. J. M.; Rowan, A. E. Do enzymes sleep and work? *Chem. Commun.* **2006**, *327*, 935−936.
(29) Klinman, J. P.; Offenbacher, A. R.; Hu, S. Origins of Enzyme Catalysis: Experimental Findings for C-H Activation, New Models, and Their Relevance to Prevailing Theoretical Constructs. *J. Am. Chem. Soc.* **2017**, *139*, 18409−18427.
(30) Edman, L.; Földes-Papp, Z.; Wennmalm, S.; Rigler, R. The fluctuating enzyme: a single molecule approach. *Chem. Phys.* **1999**, *247*, 11−22.
(31) English, B. P.; Min, W.; van Oijen, A. M.; Lee, K. T.; Luo, G.; Sun, H.; Cherayil, B. J.; Kou, S. C.; Xie, X. S. Ever-fluctuating single enzyme molecules: Michaelis-Menten equation revisited. *Nat. Chem. Biol.* **2006**, *2*, 87−94.
(32) Iversen, L.; Tu, H.-L.; Lin, W.-C.; Christensen, S. M.; Abel, S. M.; Iwig, J.; Wu, H.-J.; Gureasko, J.; Rhodes, C.; Petit, R. S.; et al. Ras activation by SOS: Allosteric regulation by altered fluctuation dynamics. *Science* **2014**, *345*, 50−54.
(33) Palmer, R. G. Broken ergodicity. *Adv. Phys.* **1982**, *31*, 669−735.
(34) Matyushov, D. V. Protein electron transfer: is biology (thermo)dynamic? *J. Phys.: Condens. Matter* **2015**, *27*, 473001.
(35) Barbara, P. F.; Meyer, T. J.; Ratner, M. A. Contemporary issues in electron transfer research. *J. Phys. Chem.* **1996**, *100*, 13148−13168.
(36) Simonson, T. Electrostatics and dynamics of proteins. *Rep. Prog. Phys.* **2003**, *66*, 737−787.
(37) Warshel, A. Dynamics of reactions in polar solvents. Semiclassical trajectory studies of electron-transfer and proton-transfer reactions. *J. Phys. Chem.* **1982**, *86*, 2218−2224.
(38) Sigfridsson, E.; Olsson, M. H. M.; Ryde, U. A comparison of the inner-sphere reaorganization energies of cytochromes, iron-sulfur clusters, and blue copper proteins. *J. Phys. Chem. B* **2001**, *105*, 5546−5552.
(39) Solomon, E. I.; Szilagyi, R. K.; DeBeer George, S.; Basumallick, L. Electronic structures of metal sites in proteins and models: Contributions to function in blue copper proteins. *Chem. Rev.* **2004**, *104*, 419−458.
(40) Cascella, M.; Magistrato, A.; Tavernelli, I.; Carloni, P.; Rothlisberger, U. Role of protein frame and solvent for the redox properties of azurin from Pseudomonas aeruginosa. *Proc. Natl. Acad. Sci. U.S.A.* **2006**, *103*, 19641−19646.
(41) Monari, A.; Very, T.; Rivail, J.-L.; Assfeld, X. A QM/MM study on the spinach plastocyanin: Redox properties and absorption spectra. *Comput. Theor. Chem.* **2012**, *990*, 119−125.
(42) Makita, H.; Hastings, G. Inverted-region electron transfer as a mechanism for enhancing photosynthetic solar energy conversion efficiency. *Proc. Natl. Acad. Sci. U.S.A.* **2017**, *114*, 9267−9272.
(43) Seyedi, S.; Matyushov, D. V. Termination of biological function at low temperatures: Glass or structural transition? *J. Phys. Chem. Lett.* **2018**, *9*, 2359−2366.
(44) LeBard, D. N.; Martin, D. R.; Lin, S.; Woodbury, N. W.; Matyushov, D. V. Protein dynamics to optimize and control bacterial photosynthesis. *Chem. Sci.* **2013**, *4*, 4127−4136.
(45) LeBard, D. N.; Matyushov, D. V. Protein-water electrostatics and principles of bioenergetics. *Phys. Chem. Chem. Phys.* **2010**, *12*, 15335−15348.
(46) Blumberger, J. Recent advances in the theory and molecular simulation of biological electron transfer reactions. *Chem. Rev.* **2015**, *115*, 11191−11238.
(47) Martin, D. R.; Matyushov, D. V. Photosynthetic diode: Electron transport rectification by wetting the quinone cofactor. *Phys. Chem. Chem. Phys.* **2015**, *17*, 22523−22528.
(48) Martin, D. R.; Matyushov, D. V. Communication: Microsecond dynamics of the protein and water affect electron transfer in a bacterial bc_1 complex. *J. Chem. Phys.* **2015**, *142*, 161101.
(49) Barragan, A. M.; Soudackov, A. V.; Luthey-Schulten, Z.; Hammes-Schiffer, S.; Schulten, K.; Solov'yov, I. A. Theoretical description of the primary proton-coupled electron transfer reaction in the cytochrome bc_1 complex. *J. Am. Chem. Soc.* **2021**, *143*, 715−723.
(50) Martin, D. R.; Matyushov, D. V. Electron-transfer chain in respiratory complex I. *Sci. Rep.* **2017**, *7*, 5495.
(51) Matyushov, D. V. Protein electron transfer: Dynamics and statistics. *J. Chem. Phys.* **2013**, *139*, 025102.
(52) Matyushov, D. V. Fluctuation relations, effective temperature, and ageing of enzymes: The case of protein electron transfer. *J. Mol. Liq.* **2018**, *266*, 361−372.
(53) Dinpajooh, M.; Martin, D. R.; Matyushov, D. V. Polarizability of the active site of cytochrome *c* reduces the activation barrier for electron transfer. *Sci. Rep.* **2016**, *6*, 28152.
(54) Cheng, J.; Terrettaz, S.; Blankman, J. I.; Miller, C. J.; Dangi, B.; Guiles, R. D. Electrochemical comparison of heme proteins by insulated electrode voltammetry. *Isr. J. Chem.* **1997**, *37*, 259−266.
(55) Wei, J. J.; Liu, H.; Niki, K.; Margoliash, E.; Waldeck, D. H. Probing electron tunneling pathways: Electrochemical study of rat heart cytochrome *c* and its mutant on pyridine-terminated SAMs. *J. Phys. Chem. B* **2004**, *108*, 16912−16917.
(56) Seyedi, S. S.; Waskasi, M. M.; Matyushov, D. V. Theory and electrochemistry of cytochrome *c*. *J. Phys. Chem. B* **2017**, *121*, 4958−4967.
(57) Matyushov, D. V.; Voth, G. A. Modeling the free energy surfaces of electron transfer in condensed phases. *J. Chem. Phys.* **2000**, *113*, 5413.
(58) Warshel, A.; Weiss, R. M. An empirical valence bond approach for comparing reactions in solutions and in enzymes. *J. Am. Chem. Soc.* **1980**, *102*, 6218−6226.
(59) Jiang, X.; Futera, Z.; Blumberger, J. Ergodicity-breaking in thermal biological electron transfer? Cytochrome *c* revisited. *J. Phys. Chem. B* **2019**, *123*, 7588−7598.
(60) Martin, D. R.; Dinpajooh, M.; Matyushov, D. V. Polarizability of the active site in enzymatic catalysis: Cytochrome c. *J. Phys. Chem. B* **2019**, *123*, 10691−10699.
(61) Feller, S. E.; MacKerell, A. D. An improved empirical potential energy function for molecular simulations of phospholipids. *J. Phys. Chem. B* **2000**, *104*, 7510−7515.
(62) Murgida, D. H.; Hildebrandt, P. Redox and redox-coupled processes of heme proteins and enzymes at electrochemical interfaces. *Phys. Chem. Chem. Phys.* **2005**, *7*, 3773−3784.
(63) Rivas, L.; Soares, C. M.; Baptista, A. M.; Simaan, J.; Di Paolo, R. E.; Murgida, D. H.; Hildebrandt, P. Electric-field-induced redox potential shifts of tetraheme cytochromes c3 immobilized on self-assembled monolayers: Surface-enhanced resonance Raman spectroscopy and simulation studies. *Biophys. J.* **2005**, *88*, 4188−4199.
(64) Marcus, R. A. Chemical and electrochemical electron-transfer theory. *Annu. Rev. Phys. Chem.* **1964**, *15*, 155−196.
(65) Levich, V. G. In *Advances in Electrochemistry and Electrochemical Engineering*; Delahay, P., Ed.; Interscience: New York, 1965; Vol. 4, pp 1−124.
(66) Chidsey, C. E. D. Free energy and temperature dependence of electron transfer at the metal-electrolyte interface. *Science* **1991**, *251*, 919−922.
(67) Schmickler, W.; Santos, E. *Interfacial Electrochemistry*, 2nd ed.; Springer: Berlin, 2010.
(68) Laviron, E. General expression of the linear potential sweep voltammogram in the case of diffusionless electrochemical systems. *J. Electroanal. Chem.* **1979**, *101*, 19−28.
(69) Compton, R. G.; Banks, C. E. *Understanding Voltammetry*; World Scientific: Singapore, 2009.
(70) Yue, H.; Khoshtariya, D.; Waldeck, D. H.; Grochol, J.; Hildebrandt, P.; Murgida, D. H. On the electron transfer mechanism

between cytochrome *c* and metal electrodes. Evidence for dynamic control at short distances. *J. Phys. Chem. B* **2006**, *110*, 19906−19913.
(71) Fried, S. D.; Boxer, S. G. Electric fields and enzyme catalysis. *Annu. Rev. Biochem.* **2017**, *86*, 387−415.
(72) Jackson, J. D. *Classical Electrodynamics*; Wiley: New York, 1999.
(73) Gitlin, I.; Carbeck, J. D.; Whitesides, G. M. Why are proteins charged? Networks of charge-charge interactions in proteins measured by charge ladders and capillary electrophoresis. *Angew. Chem.* **2006**, *45*, 3022.
(74) Zahler, C. T.; Zhou, H.; Abdolvahabi, A.; Holden, R. L.; Rasouli, S.; Tao, P.; Shaw, B. F. Direct measurement of charge regulation in metalloprotein electron transfer. *Angew. Chem., Int. Ed.* **2018**, *57*, 5364−5368.
(75) Feynman, R. P. *Statistical Mechanics*; Westview Press: Boulder, CO, 1998.
(76) Gardiner, C. W. *Handbook of Stochastic Methods*; Springer: Berlin, 1997.
(77) Matyushov, D. V. Non-Gaussian statistics of binding/unbinding events and the energetics of electron transfer reactions. *Chem. Phys.* **2008**, *351*, 46−50.
(78) Waskasi, M. M.; Martin, D. R.; Matyushov, D. V. Wetting of the protein active site leads to non-Marcusian reaction kinetics. *J. Phys. Chem. B* **2018**, *122*, 10490−10495.
(79) Solomon, E. I. Spectroscopic methods in bioinorganic chemistry: Blue to green to red copper sites. *Inorg. Chem.* **2006**, *45*, 8012−8025.
(80) Solomon, E. I.; Hare, J. W.; Dooley, D. M.; Dawson, J. H.; Stephens, P. J.; Gray, H. B. Spectroscopic studies of stellacyanin, plastocyanin, and azurin. Electronic structure of the blue copper sites. *J. Am. Chem. Soc.* **1980**, *102*, 168−178.
(81) Zheng, L.; Polizzi, N. F.; Dave, A. R.; Migliore, A.; Beratan, D. N. Where is the electronic oscillator strength? Mapping oscillator strength across molecular absorption spectra. *J. Phys. Chem. A* **2016**, *120*, 1933−1943.
(82) Phillips, J. C.; Braun, R.; Wang, W.; Gumbart, J.; Tajkhorshid, E.; Villa, E.; Chipot, C.; Skeel, R. D.; Kalé, L.; Schulten, K. Scalable molecular dynamics with NAMD. *J. Comput. Chem.* **2005**, *26*, 1781−1802.
(83) Ayala, R.; Sprik, M. A classical point charge model study of system size dependence of oxidation and reorganization free energies in aqueous solution. *J. Phys. Chem. B* **2008**, *112*, 257−269.
(84) Hummer, G.; Pratt, L. R.; García, A. E.; Berne, B. J.; Rick, S. W. Electrostatic potentials and free energies of solvation of polar and charged molecules. *J. Phys. Chem. B* **1997**, *101*, 3017−3020.
(85) Allen, M. P.; Tildesley, D. J. *Computer Simulation of Liquids*; Clarendon Press: Oxford, 1996.
(86) Matyushov, D. V. Ewald sum corrections in simulations of ion and dipole solvation and electron transfer. *J. Chem. Phys.* **2021**, *155*, 114110.
(87) Hummer, G.; Pratt, L. R.; García, A. E. Molecular theories and simulation of ions and polar molecules in water. *J. Phys. Chem. A* **1998**, *102*, 7885−7895.
(88) Hünenberger, P. H.; McCammon, J. A. Ewald artifacts in computer simulations of ionic solvation and ion-ion interaction: A continuum electrostatics study. *J. Chem. Phys.* **1999**, *110*, 1856.
(89) Nijboer, B. R. A.; Ruijgrok, T. W. On the energy per particle in three- and two-dimensional Wigner lattices. *J. Stat. Phys.* **1988**, *53*, 361−382.
(90) Murgida, D. H. In situ spectroelectrochemical investigations of electrode-confined electron-transferring proteins and redox enzymes. *ACS Omega* **2021**, *6*, 3435−3446.
(91) Hildebrandt, P.; Murgida, D. H. Electron transfer dynamics of cytochrome c bound to self-assembled monolayers on silver electrodes. *Bioelectrochemistry* **2002**, *55*, 139−143.
(92) Yamamoto, H.; Liu, H.; Waldeck, D. H. Immobilization of cytochrome c at Au electrodes by association of a pyridine terminated SAM and the heme of cytochrome. *Chem. Commun.* **2001**, *0*, 1032−1033.
(93) Chi, Q.; Zhang, J.; Andersen, J. E. T.; Ulstrup, J. Ordered assembly and controlled electron transfer of the blue copper protein azurin at gold (111) single-crystal substrates. *J. Phys. Chem. B* **2001**, *105*, 4669−4679.
(94) Uğurbil, K.; Mitra, S. 1H NMR studies of electron exchange rate of Pseudomonas aeruginosa azurin. *Proc. Natl. Acad. Sci. U.S.A.* **1985**, *82*, 2039−2043.
(95) Richert, R.; Gabriel, J. P.; Thoms, E. Structural relaxation and recovery: A dielectric approach. *J. Phys. Chem. Lett.* **2021**, *12*, 8465−8469.

https://doi.org/10.1021/acs.jpcb.2c00338
J. Phys. Chem. B 2022, 126, 3000−3011